# Analysis of wavefront propagation using the Talbot effect

Ping Zhou and James H. Burge*

College of Optical Sciences, University of Arizona, Tucson, Arizona 85721, USA

*Corresponding author: jburge@optics.arizona.edu

Received 19 May 2010; revised 20 August 2010; accepted 31 August 2010;
posted 3 September 2010 (Doc. ID 128711); published 24 September 2010

Talbot imaging is a well-known effect that causes sinusoidal patterns to be reimaged by diffraction with characteristic period that varies inversely with both wavelength and the square of the spatial frequency. This effect is treated using the Fresnel diffraction integral for fields with sinusoidal ripples in amplitude or phase. The periodic nature is demonstrated and explained, and a sinusoidal approximation is made for the case where the phase or amplitude ripples are small, which allows direct determination of the field for arbitrary propagation distance. Coupled with a straightforward method for calculating the effect in a diverging or converging beam, the Talbot method provides a useful approximation for a class of diffraction problems. 

*OCIS codes:* 050.1940, 070.6760.

## 1. Introduction

When a periodic object is illuminated by coherent light, an exact image of the structure will appear at certain distances by free-space propagation. This phenomenon is known as the Talbot effect [1] or self-imaging, which is a typical Fresnel or near-field diffraction. In Fresnel diffraction, the spherical waves arising from point sources in the aperture are approximated as quadratic-phase surfaces. When collimated light illuminates the periodic object, the self-image planes are equispaced and well defined. If the object has a period of $p$ and the wavelength of the illumination is $\lambda$, then the self-images are formed in planes, which are multiples of the Talbot distances $z_T = 2p^2/\lambda$. The Talbot distance is valid for collimated illumination. For spherical illumination, the replication of the object is amplified and the distance between the self-image planes varies with propagation.

Besides those self-image planes, the diffraction field at any distance behind the periodic object is of interest to many researchers. Winthrop and Worthington [2] describe the diffraction pattern of periodic objects as the superposition of certain replicas of the initial objects using the Fresnel–Kirchhoff formulation. Each replica of the object is shifted laterally and modulated in amplitude and phase by a constant coefficient, which is obtained from a series of complex numbers. Ojeda-Castaneda and Sicre [3] and Testorf and Ojeda-Castaneda [4] discussed the Talbot effect using the Wigner distribution function (WDF), which provides a link between Fourier optics and geometrical optics. Their approach allows calculating the field distribution at a fractional Talbot distance. Lu and Zhou use the finite-difference time-domain (FDTD) method to analyze the field distribution at any plane behind the periodic object [5].

When the periodic objects have either weak phase or amplitude distribution, the calculation of the field distribution at any plane can be simplified. This paper reviews the calculation for this case using the angular spectrum method [6]. With small-angle approximation, it shows that the amplitude and phase of the electric field have fairly simple expressions: both the phase and amplitude modulation has a sinusoidal variation as a function of the propagation distance. For a wavefront with a certain spatial frequency, the Talbot effect can be used to estimate the phase and amplitude after it propagates to any distance and can greatly simplify the calculation.

0003-6935/10/285351-09$15.00/0

The Talbot distance as described above is valid only for collimated illumination. This paper presents an equivalent propagation distance that allows application of the Talbot effect in converging or diverging light. We find that the phase and amplitude modulation as the wavefront propagates depend only on the Fresnel number and the spatial frequency of the initial object.

This paper focuses on the general analysis of wavefront propagation using the Talbot effect and the simulation shows its validity. An example of the application in the metrology with interferometers is provided in our other papers [7–10].

## 2. Talbot Effect in a Collimated Beam

The Talbot effects of sinusoidal amplitude and phase gratings in collimated illumination are discussed in the next two sections. We follow the conventional Fourier analysis shown by Goodman [6] to derive the amplitude and phase distribution after the periodic structure propagates to a certain distance.

### A. Sinusoidal Amplitude Grating

Consider a one-dimensional (1-D) sinusoidal amplitude field distribution with a period of $p$ and magnitude of variation $\alpha$, which could be created by uniform illumination upon a grating with sinusoidal transmission:

$$u(x) = 1 + \alpha \sin\left(\frac{2\pi x}{p}\right). \tag{1}$$

This treatment neglects edge effects, assuming a continuous function over $x = (-\infty, +\infty)$. The angular spectrum of this amplitude grating can be obtained by taking a Fourier transform of $u(x)$:

$$U_{z=0}(\xi) = \delta(\xi) + \frac{1}{2} j\alpha[\delta(\xi + \xi_0) - \delta(\xi - \xi_0)], \tag{2}$$

where $\xi$ is the spatial frequency, $j$ is the imaginary unit, and $\delta$ is the delta function. This angular spectrum is nothing more than three plane-wave beams with appropriate direction and phase. The diffraction pattern after propagating a distance $z$ can be calculated by multiplying its angular spectrum $U_{z=0}(\xi)$ with the free-space transfer function $H_z(\xi)$ and then taking an inverse Fourier transform [6]. If the period of the grating is very large compared to the wavelength $\lambda$, the free-space transfer function is

$$H_z(\xi) = e^{j\frac{2\pi z}{\lambda}\sqrt{1-(\lambda\xi)^2}} \approx e^{j\frac{2\pi z}{\lambda}} e^{-j\pi z\lambda\xi^2}. \tag{3}$$

Applying the free-space transfer function to $U_{z=0}(\xi)$ gives

$$\begin{aligned} U_z(\xi) &= e^{j\frac{2\pi z}{\lambda}}\left\{\delta(\xi) + \frac{1}{2} j\alpha e^{-j\pi z\lambda\xi_0^2}[\delta(\xi + \xi_0) - \delta(\xi - \xi_0)]\right\} \\ &= e^{j\frac{2\pi z}{\lambda}}\left\{\delta(\xi) + \frac{1}{2} j\alpha[\cos(\pi z\lambda\xi_0^2)\right. \\ &\quad \left. - j\sin(\pi z\lambda\xi_0^2)][\delta(\xi + \xi_0) - \delta(\xi - \xi_0)]\right\}. \end{aligned} \tag{4}$$

By dropping the constant phase term $e^{j\frac{2\pi z}{\lambda}}$ at any plane, the diffraction field after propagating a distance of $z$ can be given by taking an inverse Fourier transform of $U_z(\xi)$:

$$\begin{aligned} u_z(x) &= 1 + \alpha[\cos(\pi z\lambda\xi_0^2) - j\sin(\pi z\lambda\xi_0^2)]\sin\left(\frac{2\pi x}{p}\right) \\ &= 1 + \alpha\cos(\pi z\lambda\xi_0^2)\sin\left(\frac{2\pi x}{p}\right) \\ &\quad - j\alpha\sin(\pi z\lambda\xi_0^2)\sin\left(\frac{2\pi x}{p}\right). \end{aligned} \tag{5}$$

If this complex field is written in the form of the amplitude and phase $u_z(x) = A_z(x)e^{i\psi_z(x)}$, then the amplitude is the square root of the imaginary and real parts. If the amplitude is described with a Taylor series in $\alpha$,

$$\begin{aligned} A_z(x) &= \sqrt{1 + 2\alpha\cos(\pi z\lambda\xi_0^2)\sin\left(\frac{2\pi x}{p}\right) + \alpha^2\sin^2\left(\frac{2\pi x}{p}\right)} \\ &\approx 1 + \alpha\cos\left(\frac{2\pi z}{z_T}\right)\sin\left(\frac{2\pi x}{p}\right) \\ &\quad + \frac{1}{2}\alpha^2\sin^2\left(\frac{2\pi z}{z_T}\right)\sin^2\left(\frac{2\pi x}{p}\right) + \ldots, \end{aligned} \tag{6}$$

and the phase is the arctangent of the ratio of the imaginary part to the real part and its Taylor series in $\alpha$ is

$$\begin{aligned} \psi_z(x) &= \arctan\left[\frac{-\alpha\sin(\pi z\lambda\xi_0^2)\sin\left(\frac{2\pi x}{p}\right)}{1 + \alpha\cos(\pi z\lambda\xi_0^2)\sin\left(\frac{2\pi x}{p}\right)}\right] \\ &\approx -\alpha\sin\left(\frac{2\pi z}{z_T}\right)\sin\left(\frac{2\pi x}{p}\right) \\ &\quad + \frac{1}{2}\alpha^2\sin\left(\frac{4\pi z}{z_T}\right)\sin^2\left(\frac{2\pi x}{p}\right) + \ldots, \end{aligned} \tag{7}$$

where $z_T$ is the Talbot distance and $z_T = 2p^2/\lambda$. Up to this point, the only approximation we have made is to assume that the period of the grating is larger than the wavelength. If we make another assumption, that this grating has a small variation in amplitude relative to the mean ($\alpha \ll 1$), then the higher order terms of the Taylor series in Eqs. (6) and (7) can be ignored. By only keeping the linear term of $\alpha$ in both $A_z(x)$ and $\psi_z(x)$, it shows that the variation

of the amplitude $A'$ follows a cosine function with the propagation distance:

$$A' \approx \alpha \cos\left(2\pi \frac{z}{z_T}\right). \tag{8}$$

Also, the amplitude ripples create phase ripples and the magnitude of the phase $W'$ (in waves) follows a sinusoidal function with propagation distance:

$$W' = -W \sin\left(2\pi \frac{z}{z_T}\right) = -\frac{\alpha}{2\pi} \sin\left(\frac{\pi z \lambda}{p^2}\right), \tag{9}$$

where $\alpha = 2\pi W$, the amplitude of the sinusoidal phase ripple in radians. At a distance $z = \frac{nz_T}{2}$ ($n$ is an integer), the diffraction pattern has pure amplitude variation; at a distance $z = \frac{(2n+1)z_T}{4}$, the diffraction pattern has constant amplitude and pure phase variation. For a weak amplitude grating, the amplitude and phase follow a cosine and a sine function, respectively, as the beam propagates. This simple conclusion is useful and helps estimate the amplitude and phase after the beam propagates to any plane. The more general case is also interesting because the harmonics are also periodic with higher frequency. So propagation of a full Talbot cycle for the fundamental coincides with integral numbers of periods for the harmonics. Talbot imaging does not require the small amplitude approximation, but the simplification that allows calculation of the field at arbitrary propagation distances does.

### B. Sinusoidal Phase Grating

A 1-D pure sinusoidal phase grating with a period of $p$ and magnitude of $W$ in waves illuminated by a collimated beam can be described as an infinite sum of Bessel functions [6]:

$$u_{z=0}(x) = e^{j\alpha \sin\left(\frac{2\pi x}{p}\right)} = \sum_{q=-\infty}^{+\infty} J_q(\alpha) \cdot e^{j\frac{2\pi q x}{p}}, \tag{10}$$

where $\alpha = 2\pi W$ in radians. By following the procedure described for the amplitude grating [Eqs. (2)–(5)], the diffraction field, after propagating a distance of $z$, can be calculated as

$$u_z(x) = \sum_{q=-\infty}^{+\infty} J_q(\alpha) \cdot e^{-j\pi z \lambda \left(\frac{q}{p}\right)^2} \cdot e^{j2\pi x \frac{q}{p}}. \tag{11}$$

The field distribution at any plane $z$ is an infinite sum of Bessel functions. If we make the same assumption, that the phase ripple is much less than 1 rad ($\alpha \ll 1$), then we can approximate the field distribution at any plane $z$ by looking only at the lower orders Bessel functions. If $\alpha \geq 1$, then the higher order Bessel functions may be larger than the lower order ones and cannot be neglected.

When $\alpha \ll 1$, the sinusoidal phase described in Eq. (10) can be simplified to

$$u_{z=0}(x) = e^{j\alpha \sin\left(\frac{2\pi x}{p}\right)} \approx 1 + j\alpha \sin\left(\frac{2\pi x}{p}\right) - \frac{\alpha^2}{2} \sin^2\left(\frac{2\pi x}{p}\right) + \ldots, \tag{12}$$

and the field distribution at the plane $z$ becomes

$$u_z(x) = 1 - \frac{\alpha^2}{4} + j\alpha \cdot e^{-j\frac{\pi z \lambda}{p^2}} \sin\left(\frac{2\pi x}{p}\right) + \frac{\alpha^2}{4} \cdot e^{-j\frac{4\pi \lambda z}{p^2}} \cos\left(\frac{4\pi x}{p}\right). \tag{13}$$

The phase of this field can be given in terms of the Taylor series expanded in $\alpha$:

$$\psi_z(x) = \alpha \cos\left(\frac{2\pi z}{z_T}\right) \sin\left(\frac{2\pi x}{p}\right) - \frac{\alpha^2}{4}\left[\sin\left(\frac{8\pi z}{z_T}\right) \cos\left(\frac{4\pi x}{p}\right) + 2 \sin\left(\frac{4\pi z}{z_T}\right) \sin^2\left(\frac{2\pi x}{p}\right)\right] + \ldots. \tag{14}$$

The Taylor series of amplitude in $\alpha$ is

$$A_z(x) = 1 - \frac{\alpha^2}{4} + \alpha \sin\left(\frac{2\pi z}{z_T}\right) \sin\left(\frac{2\pi x}{p}\right) + \frac{\alpha^2}{4}\left[\cos\left(\frac{8\pi z}{z_T}\right) \cos\left(\frac{4\pi x}{p}\right) + 2 \cos^2\left(\frac{2\pi z}{z_T}\right) \sin^2\left(\frac{2\pi x}{p}\right)\right] + \ldots. \tag{15}$$

The term quadratic in $\alpha$ corresponds to the second harmonics, and they have much smaller magnitude because $\alpha \ll 1$. By keeping only the term linear in $\alpha$, the phase reduces to

$$\psi_z(x) = \alpha \cos\left(2\pi \frac{z}{z_T}\right) \sin\left(\frac{2\pi x}{p}\right), \tag{16}$$

and the amplitude becomes

$$A_z(x) = 1 + \alpha \sin\left(2\pi \frac{z}{z_T}\right) \sin\left(\frac{2\pi x}{p}\right). \tag{17}$$

Again, the harmonics are periodic with integral number of cycles within one Talbot cycle, so the Talbot imaging phenomenon remains valid for large phase ripples. As a sinusoidal phase pattern propagates, it will cycle through a reverse contrast amplitude pattern, a conjugate phase pattern, a pure amplitude pattern, and then back to the original phase pattern.

Compared to the original phase ripple, the magnitude of the phase ripple is approximately modulated by a cosine function. If the magnitude of the original phase ripple is $W$ in waves, then the attenuation of the phase ripple as it propagates a distance $z$ can be described as

$$W' = W\cos\left(2\pi\frac{z}{z_T}\right) = W\cos\left(\frac{\pi z\lambda}{p^2}\right). \quad (18)$$

For many applications, this propagation distance is small compared to the Talbot distance. In this case,

$$W' \approx W\left(1-\frac{\pi^2\lambda^2 z^2}{2p^2}\right). \quad (19)$$

The magnitude of the phase becomes smaller than (if not equal to) that of the original phase. We call this the phase smoothing effect. The pure phase ripples also create amplitude ripples accordingly, which have a sinusoidal distribution, as shown in Eq. (17).

In conclusion, for a wavefront with periodic, weak amplitude or phase variations, the Talbot effect behaves as expected, with the periodic cycling between amplitude and phase. While the periodic behavior is general, we show that this behavior is approximated as sinusoidal for cases with amplitude ripples much less than the mean, or phase ripples much less than 1 rad. In general, higher harmonics are generated, which are about a factor of $\alpha$ less than the fundamental where $\alpha$ is the ratio of the amplitude variation to the mean, or it is the amplitude of phase ripples in units of radians.

Note that the Talbot analysis is for one single frequency, but the method is general, because any distribution can be decomposed into a set of sinusoidal functions. The propagation using the Talbot analysis allows us to take advantage of the linear behavior of diffraction. Since the Fourier components do not interact, we decompose the distribution into Fourier components, then propagate each component with a simple transfer function. The resulting distribution can be reconstructed by integrating over the Fourier space.

### 3. Physical Insight of the Talbot Effect

When the periodic object has weak phase or amplitude distribution, the Talbot effect can be understood in terms of three-beam interference [11]. The form of Eq. (2) is that of three plane waves (the three lowest harmonics of the object), as shown in Fig. 1. One plane wave propagates along the $z$ axis, and the other two are off-axis and symmetric about the $z$ axis. The resulting field is the addition of these three plane waves. This three-beam interference causes the amplitude and phase to vary periodically in space. At the Talbot distance, the pattern is the same as the original one. The pattern is shifted sideways at the half-Talbot distance.

The simplicity of three-beam interference helps understand the physics of the Talbot effect, and

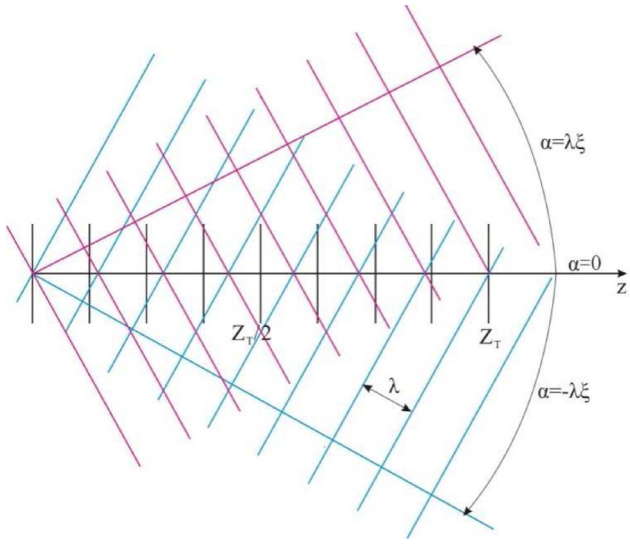


Fig. 1. (Color online) Talbot effect illustrated as three-beam interference. The angular spectrum of a laser beam transmitted through a periodic object consists of three plane waves, which combine together to form the periodic replication of the original periodic structure along the $z$ axis.

the self-imaging effect can be simulated as a sum of three plane waves. Consider a phase ripple with amplitude of $0.05\lambda$; the phase and amplitude distributions for propagating the Talbot distance two times are simulated using the method of the three-beam interference, as shown in Fig. 2. The replication of the original wavefront can be obtained by simply adding the complex amplitude of the three plane waves.

### 4. Talbot Effect in a Spherical Converging or Diverging Beam

In some applications, the periodic structure propagates in a spherical beam [12]. The field distribution of a periodic structure propagating in a spherical beam can be obtained using the Fresnel–Kirchhoff integral or other approaches [13,14,12]. Those approaches require extensive mathematical treatment. In this paper, we present an equivalent propagation method for the weak periodic structure that allows calculating the phase and amplitude distribution with the simple expressions derived in Section 2.

The Talbot distance $z_T$ is defined for a collimated light. For a spherical beam, it is convenient to convert it into an equivalent collimated beam and then use the Talbot effect to predict how wavefronts change due to propagation. The diffraction pattern for a spherical beam is the same as that observed for a collimated beam, except that the diffraction pattern occurs at the *effective propagation distance* $L_e$, and it is scaled in the transverse dimension.

As shown in Fig. 3, a converging wavefront starting with radius of curvature $R_1$, diameter $2a_1$, and ripples with period $p_1$, propagates to a position where it has radius of curvature $R_2$. To convert this propagation to equivalent propagation in a collimated space, an ideal lens with an arbitrary focal length

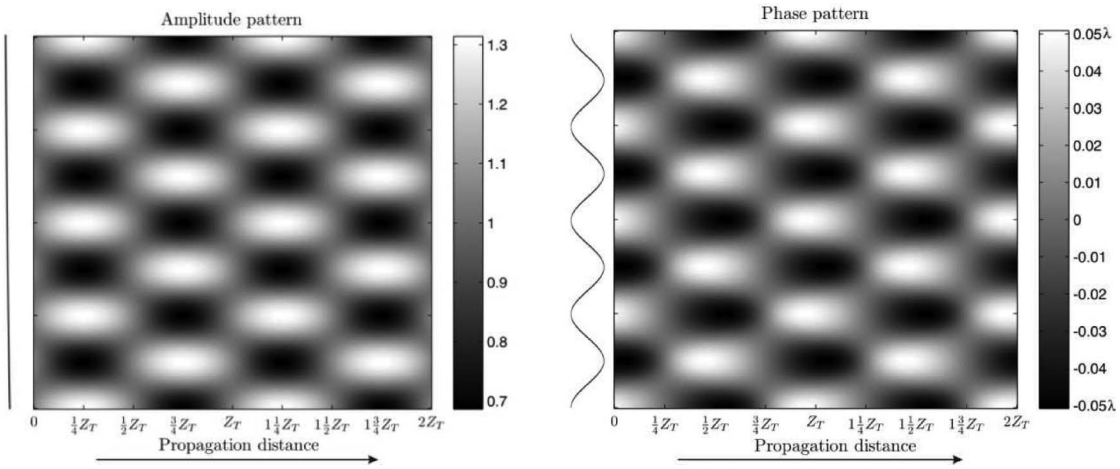


Fig. 2. Simulation of the phase and amplitude distribution using the method of three-beam interference. The original phase ripple has an amplitude of $0.05\lambda$.

$f$ is used to convert the light into collimated light. Then we use geometric imaging relationships to calculate equivalent dimensions. Assuming an ideal imaging system, the amplitude and phase variations are correctly imaged through the lens.

In collimated space, the equivalent propagation distance is

$$\Delta Z' = Z_2' - Z_1' = f^2\left(\frac{1}{R_2} - \frac{1}{R_1}\right), \tag{20}$$

and the phase ripple has a period of

$$p' = \frac{f}{R_1} p_1. \tag{21}$$

The attenuation of the phase ripple due to propagation, via Eq. (18), in the equivalent collimated space becomes

$$W' = W \cdot \cos\left(\frac{\pi\lambda \cdot \Delta Z'}{p'^2}\right) = W \cdot \cos\left(\frac{\pi\lambda R_1 \cdot (R_1 - R_2)}{R_2 \cdot p_1^2}\right). \tag{22}$$

The focal length $f$ in Eq. (22) falls off, and this makes sense because the lens is arbitrarily selected to convert a spherical beam to a collimated one. Comparing Eq. (22) with Eq. (18) shows that $\frac{R_1(R_1-R_2)}{R_2}$ is equivalent to $z$. Therefore, the effective propagation distance $L_e$ can be defined as

$$L_e = \frac{R_1(R_1 - R_2)}{R_2}, \tag{23}$$

and Eq. (22) becomes

$$W' = W \cdot \cos\left(\frac{\pi\lambda \cdot L_e}{p_1^2}\right). \tag{24}$$

The period of the phase ripple $p$ varies as it propagates in a spherical beam. To avoid the scaling issue, the ripple period can be normalized by $2a$, the diameter of the aperture. Thus, the normalized frequency $f_{\text{normalized}} = 2a_1/p_1$ [cycles/diameter], remains unchanged as the wavefront propagates in any type of illumination. By replacing the period $p_1$ with the normalized frequency $f_{\text{normalized}}$, Eq. (24) becomes

$$W' = W \cos\left(\frac{\pi\lambda L_e f_{\text{normalized}}^2}{4a_1^2}\right). \tag{25}$$

By using the Fresnel number $N_f$,

$$N_f = \frac{a_1^2}{\lambda L_e}, \tag{26}$$

Eq. (25) can be further reduced to

$$W' = W \cos\left(\frac{\pi f_{\text{normalized}}^2}{4N_f}\right). \tag{27}$$

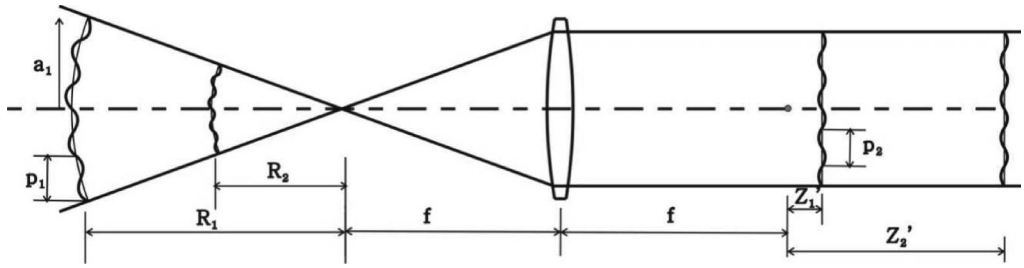


Fig. 3. Propagation in a converging space is converted to equivalent propagation in a collimated space.

Physically, the Fresnel number represents the geometric difference between the distance from the edge of the aperture to the observation point, and the distance from the center of the aperture to the observation point, divided by $\lambda/2$. Equation (27) shows that the phase smoothing effect of the periodic structure depends only on the Fresnel number, which is a function of effective propagation distance, aperture size, and wavelength. The larger the Fresnel number, the less the smoothing effect is. For any given geometry, the Fresnel number can be calculated, allowing the change of the wavefront magnitude due to propagation to be estimated at any given frequency. A transfer function describing the magnitude of the phase smoothing can be defined as

$$TF = \frac{W'}{W} = \cos\left(\frac{\pi f^2_{\text{normalized}}}{4N_f}\right). \tag{28}$$

Another useful form of the transfer function is to describe it in terms of $F$-number, which is $\frac{R_1}{2a_1}$ in this case. Rewrite Eq. (21) with $F$-number and normalized spatial frequency, and we have

$$TF = \cos\left(\frac{\pi\lambda\cdot\Delta Z'}{p'^2}\right) = \cos\left(\frac{\pi\lambda R_1^2}{p_1^2}\left(\frac{1}{R_2}-\frac{1}{R_1}\right)\right)$$
$$= \cos\left(\pi\lambda F_n^2 f^2_{\text{normalized}}\left(\frac{1}{R_2}-\frac{1}{R_1}\right)\right). \tag{29}$$

Note that the phase attenuation varies with spatial frequency. In general, any wavefront aberration can be decomposed to a collection of sinusoidal ripples with variable spatial frequencies. For each frequency component, the phase attenuation can be estimated by the transfer function.

As mentioned in Subsection 2.B, the amplitude variation follows a sine function as a periodic structure propagates in a collimated beam. In spherical illumination, the irradiance varies proportional to the inverse beam size as the beam propagates. The amplitude variation will follow a sine function if it is scaled by the beam size ($\frac{1}{R^2}$).

The transfer function shows how wavefront irregularities with high spatial frequency are filtered by propagation. This is of great importance to interferometry, where the high-frequency phase information is needed. As an example, Fig. 4 shows a phase transfer function due to a defocused image plane for an interferometric measurement of a 50 mm optic with a defocus error of 500 mm. It is clear that this defocus causes loss of information (phase smoothing) for a frequency above 40 cycles/diameter (period of 1.25 mm) and causes severe problems for higher frequencies, which can show phase reversal at about 90 cycles/diameter (period of 0.56 mm).

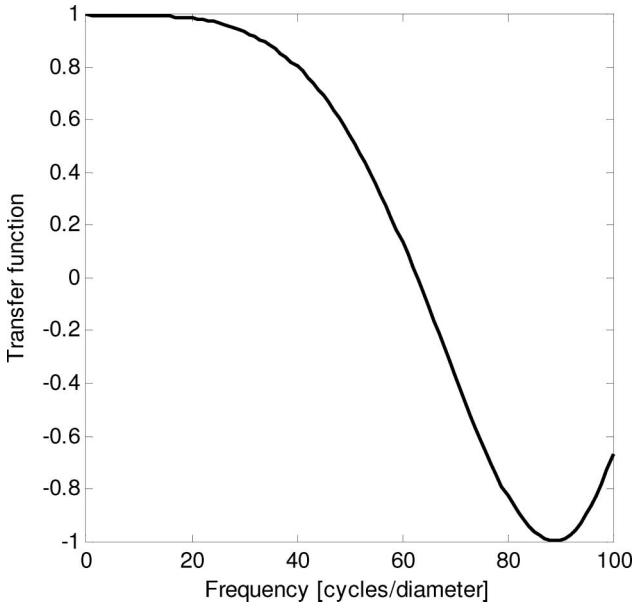

Fig. 4. Transfer function due to a defocused image plane for interferometric measurement of a 50 mm optic with 500 mm defocus error. The wavelength is 632.8 nm. The defocus causes loss of information (phase smoothing) for a frequency above 40 cycles/diameter and causes severe problems for higher frequencies, which show phase reversal.

## 5. Edge Diffraction

The analysis above neglects all edge effects. Edge diffraction occurs when the wavefront strikes the edge of an aperture, which acts as a secondary source and creates a new wavefront. The new wavefront propagates into the geometric shadow of the aperture and looks like diffraction "ripples" around the edge of the aperture [13,15]. It will also be seen when an aperture is not in focus in an imaging system. The edge diffraction pattern can be studied by dividing the aperture into Fresnel zones and calculating the Fresnel number. The severity of the edge diffraction depends on the Fresnel number, which is a function of the wavelength and propagation distance. A larger Fresnel number (closer to the periodic structure) means less edge diffraction. The edge diffraction becomes more significant as the Fresnel number becomes small (further away from the periodic structure).

The diffraction near the edge of the aperture can be modeled as Fresnel knife-edge diffraction. The real and imaginary parts of the electric field distribution can be found by evaluating the Fresnel integrals [13]. Figure 5 shows the amplitude and phase fluctuations due to edge diffraction. Both amplitude and phase have rapid oscillations as the distance from the edge becomes large. The central 80% of the aperture will be virtually free of edge effects when the distance from the edge corresponding to 10% of the aperture radius is $5(\lambda L_e/2)^{1/2}$ (about six ripples from the edge), or

$$5\sqrt{\frac{\lambda L_e}{2}} < 0.1a, \qquad N_f = \frac{a^2}{\lambda L_e} > 1250. \tag{30}$$

The Fresnel number of the geometry has to be greater than 1250 in order to have six or more ripples

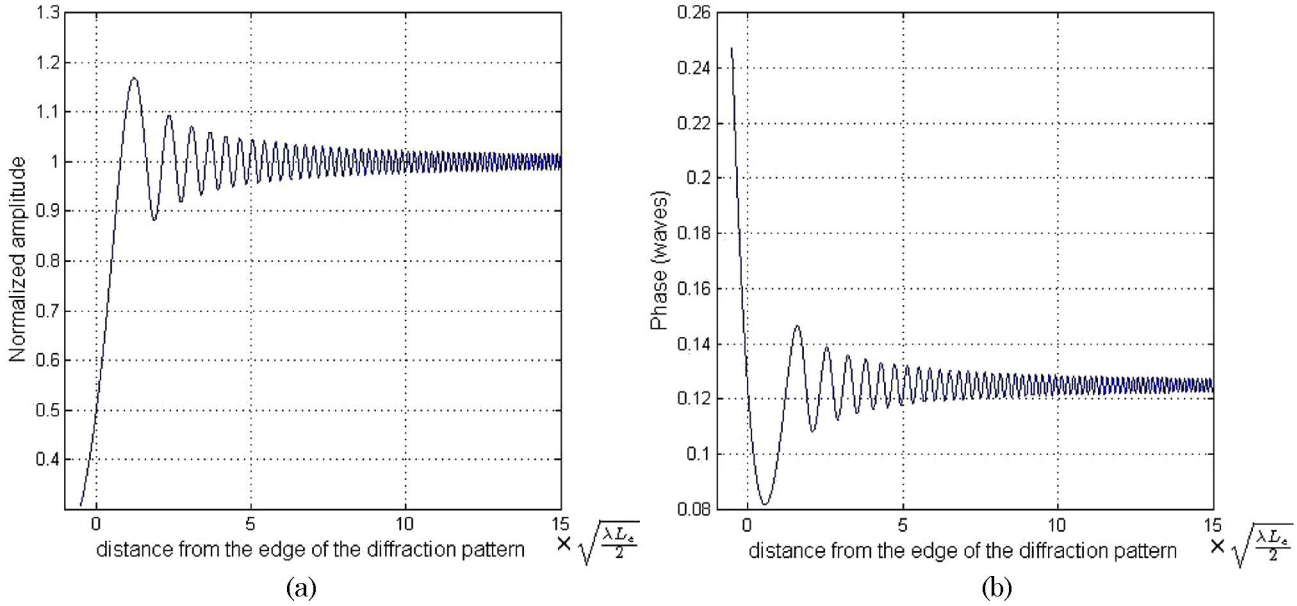


Fig. 5. (Color online) (a) Amplitude and (b) phase variation from a knife edge.

at 10% of the aperture radius from the edge. In addition, the period under consideration should be long enough that the Fresnel number for propagation is larger than the number of ripples across the aperture. Otherwise, the edge diffraction effect will strongly interact with the Talbot effect of the periodic structures.

Figure 6 shows the period of the edge diffraction ripples, the amplitude envelop, and the phase envelop, which drop quickly with respect to the distance from the edge of the diffraction pattern. It is interesting to note that the three curves have exactly the same shape and they can be obtained one from the other by only scaling and translating.

Edge diffraction is often seen in interferometry. There are many apertures inside an interferometer that cannot be in focus because interferometers often image the surface under test on the detector to correctly represent the errors in the test surfaces. Edge diffraction from the limiting aperture usually has the most dominant effect in a measurement, like the transmission sphere/flat.

## 6. Simulation

To verify the equations derived above for calculating the phase and amplitude behind a weak periodic structure, a simulation, based on wave propagation, was performed using the physical model of the ASAP, an optical modeling software [16].

A sinusoidal phase ripple with a magnitude of $\pm 0.05\lambda$ ($m = 0.31$ rad) and the amplitude of unity propagates one Talbot distance in the collimated beam. The phase and amplitude distribution are plotted in Fig. 7. The analytical solution is obtained using the Eqs. (17) and (18). They agree with the ASAP simulation.

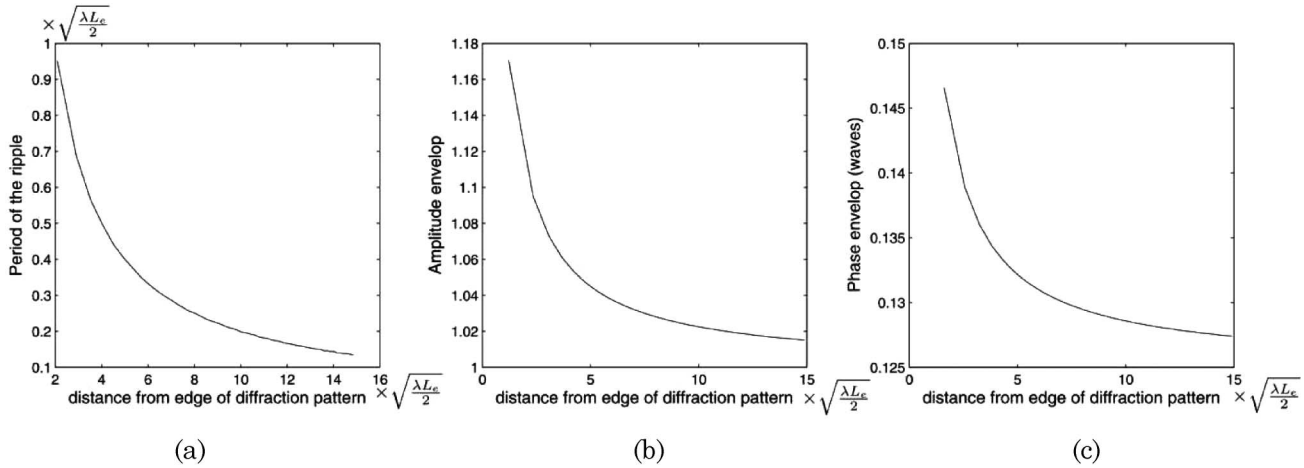


Fig. 6. (a) Period of the edge diffraction ripples, (b) the amplitude envelop, and (c) the phase envelop due to edge diffraction.

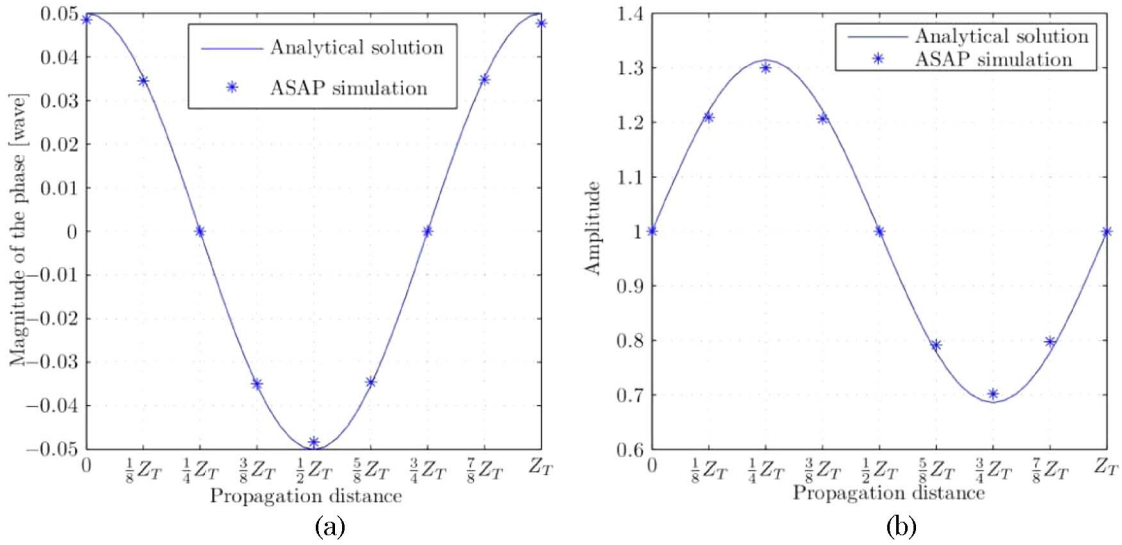


Fig. 7. (Color online) (a) Phase and (b) amplitude distribution at $x = 0$ as a weak phase ripple propagates one Talbot distance. The results from the Fourier analysis were validated with numerical simulation using ASAP.

Numerical simulation using ASAP was also used to verify the effective propagation distance for a converging spherical beam. If a spherical wavefront ($\lambda = 0.5\ \mu$m) starting with radius of curvature 20 mm and diameter 2 mm passes through a sinusoidal phase grating with period 0.1 mm, the $\frac{z_T}{8}$, $\frac{z_T}{4}$, $\frac{z_T}{2}$, $\frac{3z_T}{4}$, and $z_T$ occur at 4.0, 2.7, 3.3, 2, and 1.3 mm from one another. This can be calculated by solving the

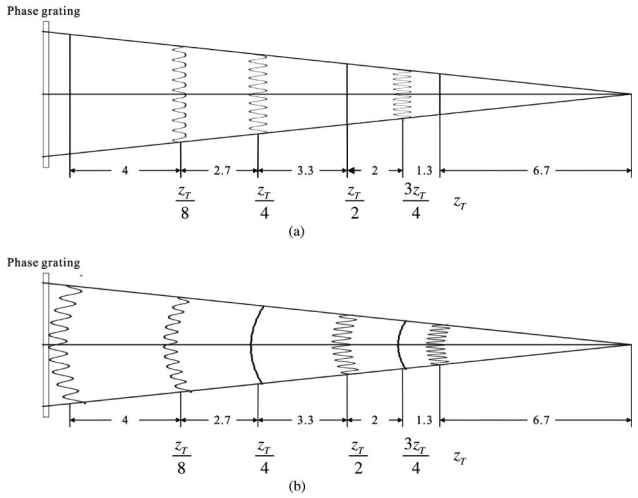


Fig. 8. (a) Amplitude and (b) phase distributions at some fractional Talbot distance in a converging spherical beam. The calculated equivalent propagation distance for converging the wavefront with a phase grating matches the simulation using ASAP. The data from the ASAP simulation are shown at appropriate propagation distances. It is clear that the results have a characteristic period defined using the equivalent propagation distance. Also, the presence of higher harmonics is seen in the nonsinusoidal shape at $z_T/8$. The amplitude variation is scaled by the inverse area in this figure, and the phase variation is also scaled to show its variation. Only ten cycles at the middle of the aperture are shown in both pictures. The numbers in the figures have units of millimeters.

$R_2$ when the effective propagation distance $L_e$ equals some fraction of the Talbot distance. An ASAP simulation is also performed to verify the calculation, and both the amplitude and phase variations are shown in Fig. 8. The data from the ASAP simulation are shown at the appropriate propagation distance.

Note that ASAP calculates the complex field in a plane instead of a sphere, so the light near the edge of the pupil propagates a longer distance than the on-axis one and there is a cosine effect. For this $F/10$ system, the cosine effect causes a propagation distance error of about 0.1%. In Fig. 8, the amplitude variation is shown on a plane where ASAP calculates the field distribution. The phase variation is shown on a curved surface. The ripples are scaled to show the phase ripples clearly.

The pure phase variation occurs right after the grating, at both the half and one Talbot distances. The pure amplitude variation happens at a quarter and three-quarters of Talbot distance. At $\frac{z_T}{8}$, there are both amplitude and phase variations. The calculated equivalent propagation distance for converging wavefront with a phase grating matches the simulation using ASAP.

## 7. Conclusion

This paper uses conventional Fourier analysis to demonstrate the Talbot effect for a sinusoidal ripple in amplitude or phase. A sinusoidal approximation is made for the case where the phase or amplitude ripples are small, which allows direct determination of the field for an arbitrary propagation distance. Coupled with a straightforward method for calculating the effect in a diverging or converging beam, the Talbot method provides a useful approximation for a class of diffraction problems. The derivation in this paper is very useful for solving or explaining the phase smoothing and edge diffraction effects in

coherent imaging systems, especially with small variations in amplitude or phase.

The authors acknowledge help from several colleagues at the College of Optical Sciences, University of Arizona: Chunyu Zhao for many discussions on this topic in general, Matt Dubin for his help with the ASAP simulation, and Tom Milster for his insight on three-beam interference. The authors also would like to thank Ulf Griesmann from the National Institute of Standards and Technology (NIST) for reading the manuscript and providing thoughtful comments. The authors are grateful for partial support from National Institute of Standards and Technology (NIST), U.S. Department of Commerce, under American Recovery and Reinvestment Act award 60NANB10D010.

## References

1. W. H. F. Talbot, "Facts relating to optical sciences. No. IV," Philos. Mag. **9**, 401–407 (1836).
2. J. T. Winthrop and C. R. Worthington, "Theory of Fresnel images. I. Plane periodic objects in monochromatic light," J. Opt. Soc. Am. **55**, 373–381 (1965).
3. J. Ojeda-Castaneda and E. E. Sicre, "Quasi ray-optical approach to longitudinal periodicities of free and bounded wavefields," Opt. Acta **32**, 17–26 (1985).
4. M. Testorf and J. Ojeda-Castaneda, "Fractional Talbot effect: analysis in phase space," J. Opt. Soc. Am. A **13**, 119–125 (1996).
5. Q. Lu and C. Zhou, "Rigorous electromagnetic analysis of Talbot effect with the finite-difference time-domain method," Proc. SPIE **5638**, 108–116 (2005).
6. J. W. Goodman, *Introduction to Fourier Optics*, 3rd ed. (Roberts, 2005).
7. C. Zhao and J. H. Burge, "Imaging aberrations from null correctors," Proc. SPIE **6723**, 67230L (2007).
8. P. Zhou, J. H. Burge, and C. Zhao, "Imaging issues for interferometric measurement of aspheric surfaces using CGH null correctors," Proc. SPIE **7790** (2010).
9. J. H. Burge, C. Zhao, and P. Zhou, "Imaging issues for interferometry with CGH null correctors," Proc. SPIE **7739**, 77390T (2010).
10. P. Zhou and J. H. Burge, "Limits for interferometer calibration using the random ball test," Proc. SPIE **7426**, 74260U (2009).
11. T. Milster, "505 Classnotes," University of Arizona, http://www.optics.arizona.edu/Milster/.
12. H. O. Carmesin and D. Goldbeck, "Depth map by convergent 3D-Talbot-interferometry," Optik (Jena) **108**, 3 (1998).
13. M. Born and E. Wolf, *Principles of Optics*, 7th ed. (Cambridge U. Press, 1999).
14. R. Jozwicki, "The Talbot effect as a sequence of quadratic phase corrections of the object Fourier transform," Opt. Acta **30**, 73–84 (1983).
15. J. B. Keller, "Geometrical theory of diffraction," J. Opt. Soc. Am. **52**, 116–130 (1962).
16. http://www.breault.com/.